

Fracture Toughness Evaluation of Powder Metallurgical ASP2030 High-Speed Steels Using Flexural Specimens and Finite Element Method

Firouzi, A.; Yazdani, S.; Tavangar, R.; Shakerifard, B.; Khan MD, F.

DOI

[10.1007/s11223-023-00482-y](https://doi.org/10.1007/s11223-023-00482-y)

Publication date

2023

Document Version

Final published version

Published in

Strength of Materials

Citation (APA)

Firouzi, A., Yazdani, S., Tavangar, R., Shakerifard, B., & Khan MD, F. (2023). Fracture Toughness Evaluation of Powder Metallurgical ASP2030 High-Speed Steels Using Flexural Specimens and Finite Element Method. *Strength of Materials*, 54 (2022)(6), 1064-1081. <https://doi.org/10.1007/s11223-023-00482-y>

Important note

To cite this publication, please use the final published version (if applicable). Please check the document version above.

Copyright

Other than for strictly personal use, it is not permitted to download, forward or distribute the text or part of it, without the consent of the author(s) and/or copyright holder(s), unless the work is under an open content license such as Creative Commons.

Takedown policy

Please contact us and provide details if you believe this document breaches copyrights. We will remove access to the work immediately and investigate your claim.

Green Open Access added to TU Delft Institutional Repository

'You share, we take care!' - Taverne project

<https://www.openaccess.nl/en/you-share-we-take-care>

Otherwise as indicated in the copyright section: the publisher is the copyright holder of this work and the author uses the Dutch legislation to make this work public.

Time-Dependent Evolution of Volume Fraction and Stability of Retained Austenite in a Hot-Rolled and Intercritically Annealed Al-Alloyed Medium-Mn Steel



ADAM SKOWRONEK , ADAM GRAJCAR , CARLOS GARCIA-MATEO , JOSÉ A. JIMÉNEZ , and ROUMEN H. PETROV 

The development of superior mechanical properties in medium-Mn requires the optimization of microstructural parameters such as retained austenite (RA) stability, volume fraction, and morphology. The present work explores the possibility of using a continuous annealing approach instead of conventional batch annealing to perform an intercritical annealing (IA) treatment in a hot-rolled strip of an Al-alloyed 5Mn steel. Dilatometric studies were performed at a temperature of 680 °C with soaking times ranging from 1 to 300 min to follow the microstructural changes as a function of time. The microstructures thus obtained were thoroughly characterized by means of X-ray diffraction, SEM and TEM, TEM-EDS microanalysis and EBSD phase and orientation maps. It was observed that with increasing soaking times, the volume fraction of retained austenite gradually increases, albeit at the cost of its stability. The comparison of martensite start temperatures (M_s) based on the chemical composition of austenite at 680 °C with that experimentally obtained at higher process temperature revealed the effect of the grain size on the reduction of RA stability for longer process times. Accordingly, mechanical tests results showed that the yield stress, tensile strength and hardness decrease with an increase in the IA soaking time.

<https://doi.org/10.1007/s11661-023-06998-x>
© The Author(s) 2023

I. INTRODUCTION

STEELS containing retained austenite (RA) are becoming increasingly attractive to the automotive sector, as new vehicle safety and fuel economy standards mandate the use of alloys that combine high ductility and high strength.^[1] Such strength-ductility combination may be obtained by strain-induced martensitic transformation (SIMT) of retained austenite, which

enhances strain hardening.^[2,3] The use of multiphase steels containing RA allows decreasing vehicle mass since complicated parts characterized by similar strength and stiffness may be produced from thinner but stronger metal sheets. Moreover, if some fraction of RA remains after the forming operations, it may be used for any subsequent event providing better energy absorption properties.^[4,5] Retained austenite stability is a key factor controlling the kinetics of SIMT and, therefore, the mechanical behavior of multiphase steels. It depends on numerous material and structural factors as: chemical composition,^[6] morphology,^[7] grain size,^[8] strength of surrounding phases,^[9] and even crystallographic texture.^[10] The most recent group of alloys specifically designed to have high fractions of stable RA in the microstructure are the medium-Mn steels, which are the next step development after the high manganese steels. The latter ones, despite containing fully austenitic microstructure which provided the excellent combination of properties, turned out to be too expensive to be used in the industry. Medium-Mn steels typically contain 3 to 12 wt pct of Mn with a carbon content of up to 0.2 wt pct.^[7] The addition of Mn is intended to improve the stability of the austenite by reducing the M_s temperature at a lower material cost.

ADAM SKOWRONEK and ADAM GRAJCAR are with the Department of Engineering Materials and Biomaterials, Faculty of Mechanical Engineering, Silesian University of Technology, Konarskiego 18a St., Gliwice 44-100, Poland. Contact e-mail: adam.grajcar@polsl.pl CARLOS GARCIA-MATEO and JOSÉ A. JIMÉNEZ are with the National Center for Metallurgical Research CENIM-CSIC, Av. De Gregorio del Amo 8, Madrid 28040, Spain. ROUMEN H. PETROV is with the Research Group Materials Science and Technology, Department of Electromechanical, Systems and Metal Engineering, Ghent University, Tech Lane Ghent Science park-Campus A Zwijnaarde, Technologiepark 46, Ghent 9052, Belgium and also with the Department of Materials Science and Engineering, Delft University of Technology, 3mE-TU Delft, Building 34, Mekelweg 2, Delft 2628 CD, The Netherlands.

Manuscript submitted October 27, 2022; accepted January 31, 2023.

Article published online February 20, 2023

Currently, the IA heat treatment allows obtaining the largest fraction of stable RA in the microstructure of the steel.^[7] This enables to improve their plastic properties significantly in comparison to thermomechanically processed steels.^[11,12] IA consists of a single austenitization in the $\alpha + \gamma$ region, where a wide range of phase ratio and chemical elements redistribution may be obtained. The two most important parameters of the process are austenitization temperature and soaking time. Both parameters control the austenite fraction and the diffusion range of C and Mn, which are at the same time the two most important elements in defining the stability of the RA.^[13] In general, an increase of the austenitization temperature increases the austenite fraction and accelerates its formation.^[14,15] However, there comes a point when the overall C and Mn concentration in steel and the diffusion rate cannot keep up with the rapid increase in the RA fraction, resulting in a poor stability, and favoring martensitic transformation during cooling, which deteriorates ductility. Therefore, many of the IA optimization attempts have focused on long-time batch annealing at moderate temperatures between 580 °C and 650 °C, depending on the chemical composition.^[16–19]

This heat treatment requires a lot of time and energy, and therefore, efforts should be made to optimize the use of intercritically treated medium-Mn steels in the more energy efficient continuous annealing line. For this reason, it is necessary to investigate the microstructural evolution of medium-Mn steels over a wide range of short processing times, but at elevated temperatures, to determine whether such a combination of processing T/t allows good mechanical properties to be maintained. Furthermore, the use of higher Al content in medium-Mn-containing steels not only widens but also increases the intercritical interval towards higher temperatures,^[20] thus promoting an increase of the transformation and diffusion rate.^[14] This novel approach, combining the increase of the processing temperature with an appropriate chemical design of the steel, can further shorten the duration of the IA treatment.

Additionally, an increased content of Al in medium-Mn steels widens the intercritical range towards higher temperatures,^[20] promoting increased transformation rate and faster diffusion.^[14] Such novel approaches combining the increased process temperature and proper chemical design of the steel may further shorten the IA process. Therefore, the aim of this work is to investigate the changes and dependencies in RA fraction, its stability, and the corresponding mechanical properties of Al-rich 5 pct Mn steel as a function of the soaking time.

II. EXPERIMENTAL PROCEDURE

A. Material and Heat Treatment

The chemical composition of the Al-alloyed medium-Mn steel used in this investigation is given in Table I. Chemical composition was determined by optical emission spectroscopy (OES) after hot rolling

Table I. Chemical Composition of the Steel Hot-Rolled Band Used for This Investigation

Chemical element, wt pct					
C	Mn	Al	Si	Mo	Fe-balance
0.16	4.7	1.6	0.20	0.20	93.12

and quenching at 2/3 of the sheet thickness, 4.5 mm, as the most representative area, not influenced by possible microsegregation. The addition of 1.6 wt. pct Al, whose main role in the steel is to prevent carbide precipitation, additionally causes a widening of the intercritical temperature range from 648 °C (A_{C1}) up to 924 °C (A_{C3}).^[14] Further details in the alloy design and production process steps are available in a previous work.^[14] The first stage of investigations concerning the influence of soaking temperature showed that the optimal microstructure condition containing 35 pct of stable RA were obtained at 680 °C for 60 min of process duration.^[14] This temperature was therefore adopted in the present study, where the attention is focused on the effect of the soaking time between 1 to 300 min in order to fully describe the changes and dependencies taking place in the material.

The kinetics of austenite formation during IA, and martensitic transformation upon subsequent cooling to room temperature, were studied by dilatometry using cylindrical samples of 4 mm diameter and 10 mm length in a high resolution dilatometer, Bahr 805A. This device enables to study phase transformation by monitoring the relative change in length (RCL) of the sample using a Linear Variable Differential Transducer (LVDT) in contact with fused silica pushrods. The dilatometer uses an induction coil and helium blown system to heat and cool the sample. The temperature is controlled throughout the experiment with an S-type thermocouple welded at mid length of the sample surface. The dilatometric data were analyzed according to ASTM A1033-04.

The initial martensitic microstructure present in the hot-rolled plate, was subjected to thermal treatments consisting of heating at 3 °C/s up to an IA temperature of 680 °C, then holding for 1, 5, 15, 60, 120, 300 min and finally cooling to room temperature at 60 °C/s. The evolution of ferrite and austenite fraction at the IA temperature as a function of the soaking time was calculated from dilatometric results using a method proposed in previous study.^[14]

B. Microstructural Characterization

The microstructures obtained after the different proposed IA treatments were evaluated by means of scanning electron microscopy (SEM), transmission electron microscopy (TEM), and X-ray diffraction (XRD). Specimens for SEM and XRD were prepared following standard metallographic procedures that included mechanical grinding with SiC paper up to 2000 grid and polishing with 3 and 1 μm grain size diamond paste. A final polish using a 35 nm colloidal silica suspension

(OPS) was included to ensure a flat surface with minimal deformation. For SEM observations a 3 pct Nital solution was used to etch the polished specimens for ~ 4 s at room temperature to develop the microstructural features. SEM observations were performed with a FEI Quanta FEG 450 SEM equipped with an energy-dispersive X-ray spectrometer (EDS) and an electron backscatter diffraction (EBSD) detector. As the structure present in the material exhibits lath-like morphology, the lath thickness was measured instead of the grain diameter to describe the microstructure and to understand material properties such as hardness and strain–stress relationship. RA lath thickness was determined by at least 200 linear intercepts on SEM micrographs to obtain reliable statistics. EBSD measurements were performed with SEM operating at 20 kV and a probe current of ~ 2.5 nA. All samples were tilted at 70° and observed at a working distance of 15 mm to maximize backscattered electrons. EBSD mapping has been carried out in a hexagonal scan grid on an area of about 40 × 40 μm² at step sizes of 70 nm. The OIM-TSL® data Analysis software v.7.31 has been used for data processing. A two-step clean-up procedure was performed to remove the bad data point. In a first step, it was established a grain tolerance angle of 5° and a minimum grain size greater than 2 pixels. Finally, in the second step, all points with CI (confidence index) < 0.1 were removed from the measurement as not being robust.

The volume fraction of RA was determined from the XRD patterns recorded with Co radiation (λ K α_1 = 0.1789 nm) in a Panalytical X'Pert Pro MPD diffractometer) equipped with a PIXcel 3D-detector in the different heat treated materials and in the uniform deformation area of the samples tested in tension to failure. Conventional θ to 2θ scans were performed over a 2θ range of 45 to 105 deg with a step size of 0.026 deg and scan speed of 0.6 s/step. The collected diffraction patterns were analyzed using the version 3.0 of the High Score Plus software (Panalytical). The RA fraction as well as its lattice parameter were determined using the Rietveld refinement method and the crystallographic information of ferrite and austenite.^[21] The C concentration in RA was calculated from the austenite lattice parameter using the following expression.^[22]

$$\alpha_\gamma = 3.556 + 0.0453x_C + 0.00095x_{Mn} + 0.0056x_{Al} \quad [1]$$

where α_γ is in Å, x_C , x_{Mn} and x_{Al} are elements concentration in austenite (wt pct).

The samples for XRD measurements of the RA fraction after uniaxial tensile deformation were cut from uniform deformation areas of the tensile samples.

TEM observations were performed in an S/TEM TITAN 80–300 microscope operating at 200 kV in lamellas of approx. 8 × 8 μm² cut along the rolling direction with focused ion beam (FIB). Semiquantitative microanalyses by energy-dispersive X-ray spectroscopy (EDS) using TEM were performed to evaluate changes in Mn and Al concentrations in RA as a function of the soaking time. For this goal, at least twenty measurements were done in random selected areas of different grains. From these results the theoretical M_s

temperatures were determined using the following equations.^[23–25]

$$M_s = 561 - 474 \times C - 33 \times Mn - 21 \times Mo \quad [2]$$

$$M_s = 545 - 601.2 \times (1 - \text{Exp}(-0.868 \times C)) - 34.4 \times Mn - 13.7 \times Si - 15.4 \times Mo - 1.4 \times Al \quad [3]$$

$$M_s = 273 - 545.8e^{-1.365 \times C} - 34.4 \times Mn - 7.5 \times Si + 30 \times Al \quad [4]$$

C. Mechanical Properties

The dependence of the mechanical properties with soaking time was evaluated at room temperature by means of hardness and tensile tests. Vickers hardness measurements were performed with a microhardness tester FB-700 at a load of 1 kgf. Ten measurements for each sample were taken and the mean hardness determined after discarding the two extreme values. Sub-sized flat tensile samples with a gauge length of 40, 6 mm wide and 2.5 mm thick were used. They were machined from the central part of hot-rolled sheet along the rolling direction. These samples were subjected to IA treatments at 680 °C in a Nabertherm LT15/12/P330 muffle furnace under argon atmosphere with the same holding time used in dilatometry tests. The tensile properties were determined according to ASTM E8 standard from static tensile test performed at a nominal strain rate of 10⁻³ s⁻¹ on a universal testing machine fitted with an extensometer.

III. RESULTS AND DISCUSSION

A. Formation and Chemical Stability of RA

The relative change in length (RCL) measured by dilatometry during the isothermal IA treatment at 680° C tests clearly show a progressive contraction of the sample with increasing holding time, as observed in Figure 1(a), which is mainly due to the austenite-reverted-transformation (ART) of martensite, and to a lesser extent to the dissolution of cementite particles into this phase. Medium-Mn steels are sometimes susceptible to segregation of this element during solidification and consequently the RCL measured during the IA may change from sample to sample.^[26] As the average kinetics of austenite-reverted-transformation measured in several dilatometric samples shows high consistency, it was deduced that the material used for this study does not present strong microsegregation of alloying elements. From same Figure 1(a), it is possible to deduce that RCL decreased progressively and 50 and 90 pct of the re-austenitization transformation was reached after ~ 4 min and ~ 50 min, respectively. This figure also

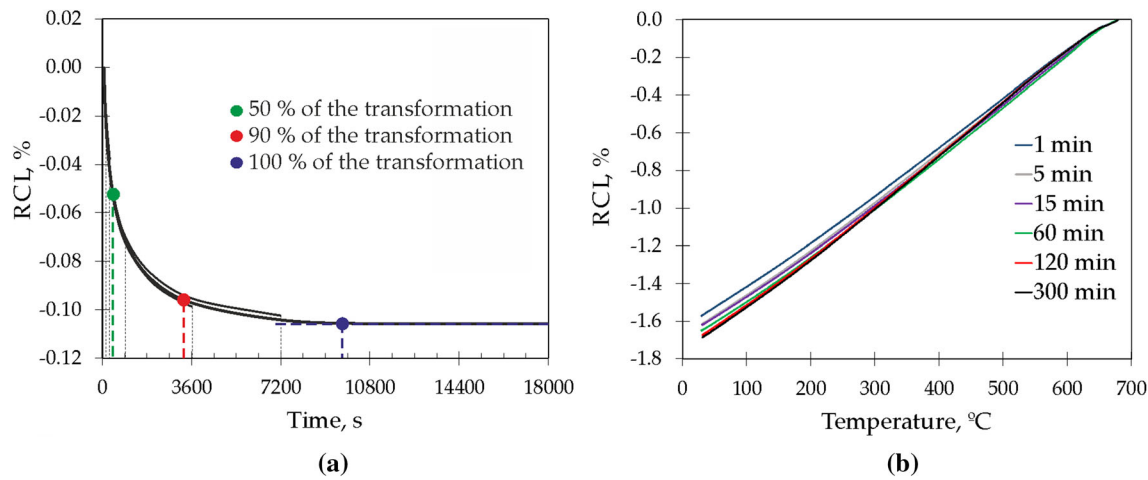


Fig. 1—Dilatometric results showing: (a) the evolution of the relative change in length (RCL) as a function of the soaking time; green, red, and violet dots mark the soaking time required to complete 50, 90 and 100 pct, respectively, of the transformation and (b) dilatometric curve, RCL, obtained on cooling to RT after the different IA treatments (Color figure online).

shows a plateau in the RCL curve after ~ 160 min associated with the completion of the transformation, which is more than 3 times longer that the time needed for an IA at 720 °C as reported in a previous study.^[14] This result shows the great importance of annealing temperature and time in the kinetics of austenite formation during IA treatments.

The austenite fraction should increase as the annealing temperature and/or time increase, and this phase must be retained at room temperature to ensure an excellent combination of strength and ductility. As shown in Figure 1(b) it is observed that regardless of the holding time used, when cooling to room temperature, the dilatometric curves remain linear and no martensitic transformation is detected in any case. The detectable differences in the slopes of the above mentioned curves are explained by the differences in the thermal expansion coefficients of the different microstructures obtained (different austenite/ferrite ratios) during the IA treatments. According to the method proposed in a previous work,^[14] the theoretical fraction of high temperature austenite has been calculated from the dilatometric curves (Figure 2(a)) and compared to the experimental data (XRD). A good agreement between the results by both methods is observed. This figure shows the retention of a considerable amount of austenite (about 16 pct) in the microstructure after just 1 min of annealing at 680 °C. The rate of transformation to austenite increases rapidly during the first 15 min (33 pct fraction), and then decreases drastically, needing ~ 160 min to reach a final fraction of ~ 41 pct.

As anticipated, the stability of RA is closely related to its carbon and manganese content, which has been determined from the austenite lattice parameter using Eq. [1] and by dispersive energy spectrometry (EDS) measurements in TEM, respectively. The measured change in concentration of both elements as a function of the soaking time is shown in Figure 2(b). The carbon concentration in RA (Figure 2(b)) is the highest after

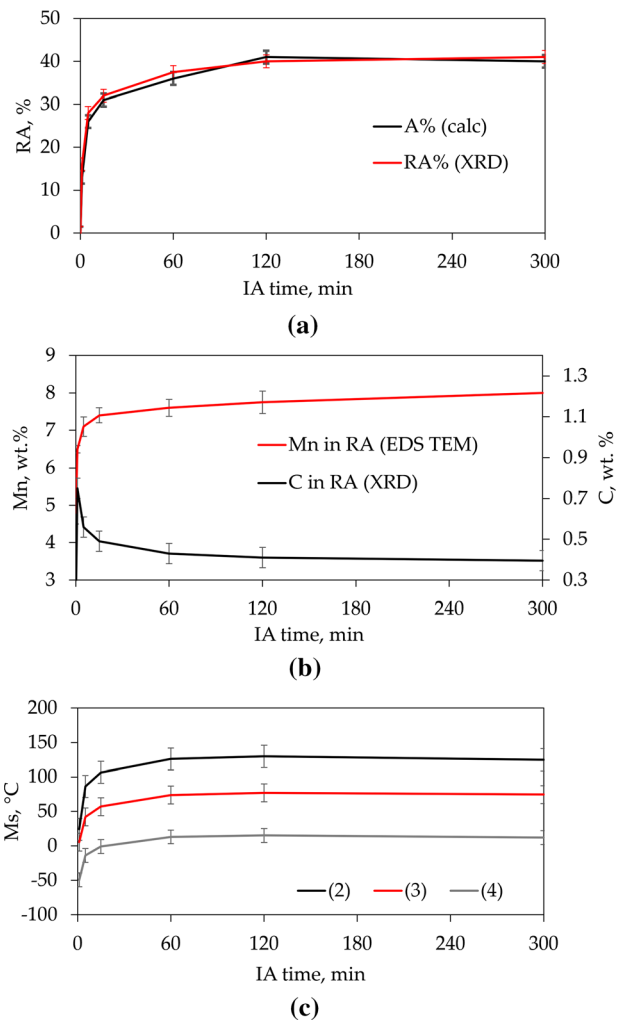


Fig. 2—Influence of the soaking time on the evolution of: (a) theoretical and experimental austenite fraction calculated from dilatometric curves and XRD data, respectively; (b) Mn and C contents in austenite determined from EDS spectra and austenite lattice parameter, respectively; and (c) M_s temperature according to Eqs. [2–4] (Color figure online).

1 min of annealing (0.74 wt pct) and decreases to 0.39 wt pct after 5 h, following the austenite formation recorded by dilatometry. The C concentration in the austenite decreases rapidly in the first 15 min of isothermal soaking up to that point. In case of the Mn concentration (Figure 2(b)), there is a sharp increase in the early stage of IA from 4.8 to 6.5 pct after just 1 min. Such intense enrichment in a short soaking time was measured also by other researchers.^[27,28] As the soaking time increases, the detected enrichment rate becomes more sluggish, reaching a Mn concentration of ~ 8 wt pct after 5 h of IA treatment. The different behavior of C and Mn partitioning can be explained by the differences in their diffusion rates, which at 680 °C for the former is much faster ($\sim 10^{-10} \text{ m}^2\text{s}^{-1}$ in ferrite and $\sim 10^{-13} \text{ m}^2\text{s}^{-1}$ in austenite)^[29] than in the latter ($\sim 10^{-16} \text{ m}^2\text{s}^{-1}$ in ferrite and $\sim 10^{-19} \text{ m}^2\text{s}^{-1}$ in austenite),^[29] therefore, enabling the C concentration to follow closely the RA fraction changes,^[30] while changes in Mn are more sluggish.^[31] Mn concentration in austenite increases slightly even after 5 h of annealing at 680 °C, while carbon achieves a maximum value and starts to drop after only 1 min.

The detected variation of C and Mn in retained austenite must reflect in its stability against martensitic transformation. Figure 2(c) shows the evolution of the M_s calculated using Eqs. [2–4] and using RA composition given in Figure 2(b). It is observed that, although the M_s values differ depending on the formula used, the overall tendency is almost identical. Despite the short soaking time, after only 1 min of soaking time austenite exhibits the highest chemical stability, lowest M_s temperature, due to the very fast enrichment in carbon (~ 0.74 pct) and manganese (~ 6.5 pct) of its relatively low fraction (16 pct). During the first 15 min of annealing the M_s temperature increases significantly which is expected to cause a drop of the thermal stability of the retained austenite. The reason is that despite the apparent increase in manganese content to 7.4 pct, the stability cannot be maintained because of fast decreasing C concentration in an increasing RA fraction (32 pct). After prolonged soaking times the mentioned interplay of fast diffusing C and slow diffusing Mn allows to maintain very similar stability of the retained austenite, M_s temperature, up to 5 h.

The M_s temperature changes presented in Figure 2(c) were calculated only on the basis of changes in the chemical composition of austenite. It should be remembered that RA stability and the M_s temperature are also influenced by other factors besides chemical composition which were mentioned in the introduction section. For this reason, another IA variant with identical process parameters but at higher IA temperature, 760 °C, was tested using dilatometry to record actual changes in M_s temperature. The calculated austenite fraction at 760 °C increases to 38 and 69 pct after 2 s and 1 h of soaking, respectively, after which it remains almost constant. At elevated temperature, all processes taking place during soaking are accelerated and austenite fraction is higher.^[14] The changes in austenite fraction are similar as at 680 °C, however, for shorter soaking time. The M_s temperature again is the lowest for the lowest RA fraction

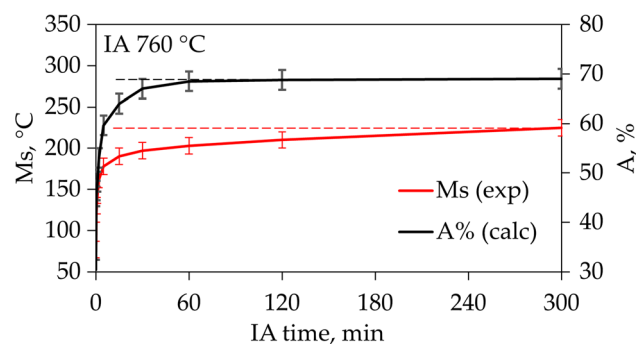


Fig. 3—The changes in austenite fraction (A) and corresponding experimental M_s at 760 °C for different soaking time determined from the dilatometric curves (Color figure online).

despite very short soaking time (2 second) and increases with soaking duration. What is important here, even after the ferrite–austenite equilibrium is obtained after 60 min of soaking treatment, is that the M_s temperature tends to continuously increase (Figure 3) with soaking time, which differs from the observed tendency at 680 °C of annealing temperature (Figure 2(c)). As measured, the C concentration follows closely changes in austenite fraction and very quickly reaches equilibrium, whereas Mn diffuses to austenite continuously (Figure 2(b)). Therefore, for constant fraction of austenite in the microstructure, the M_s temperature should also be constant or grow slightly if we consider only the influence of chemical composition of austenite. The growth tendency of experimental M_s shows the influence of factors other than chemical composition as grain size or matrix strength, on austenite stability.

The local redistribution of Mn in samples soaked at 680 °C has also been determined from EDS data obtained using a spectrometer attached to an SEM and TEM. Both, TEM elemental line profiles and SEM–EDS mappings in Figure 4 show similar evolution of the Mn content with soaking time. Clear and significant changes in manganese concentrations in ferrite and austenite regions were recorded. Manganese and carbon redistributed to the austenite, while were depleted in ferrite (Figure 4). Austenite manganese enrichment is fairly uniform in after 1 min of soaking (Figure 4(a)). By increasing the soaking time to 300 min, further increase its degree of enrichment although it became more heterogeneous, denoted by peaks of the Mn concentration profiles close to the ferrite/austenite interfaces,^[32] see Figure 4(b). This tendency is even stronger if the RA is adjacent to coarse ferritic grains and is caused by significantly faster Mn diffusion in ferrite than in austenite.^[33] A rapid depletion of even large ferrite grains into manganese and carbon occurs. However, these elements accumulate close to the austenite grain boundary, which is confirmed by other researchers.^[34]

B. Microstructure Evolution

The formation of austenite during IA of hot-rolled medium manganese steels with martensitic initial microstructure occurs in an austenite reverse

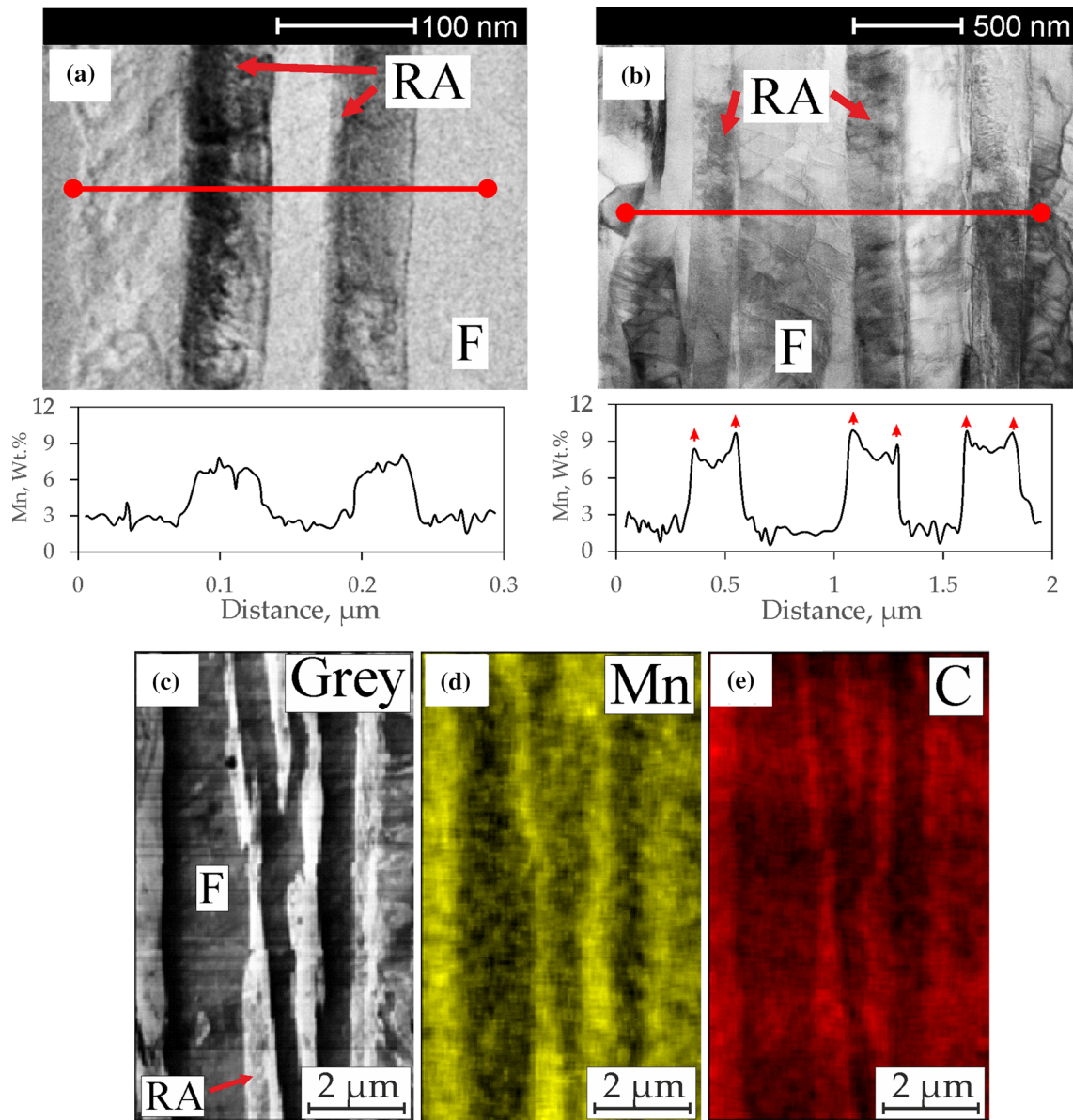


Fig. 4—EDS results: TEM micrographs with Mn elemental line obtained in sample annealed for (a) 1 min and (b) 300 min, (c) SEM micrographs of a sampled annealed for 300 min together with (d) Mn and (e) C mappings obtained in the same zone (Color figure online).

transformation (ART) mode by the growth of interlath austenite nucleated along martensite lath boundaries.^[35] The newly formed phase therefore inherits the lath-like morphology present in the parent martensite (Figure 5(a)) leading to a duplex microstructure with austenite and ferrite lamella (Figure 5(b)-(d)). As described previously, the austenite has an initial rapid growth and after 1 min of annealing a relatively high volume fraction of thin lath-like retained austenite distributed between coarse tempered martensite laths is obtained, as shown in Figure 5(b). On the other hand, this microstructure also included a significant amount of carbide particles precipitated in the central area and at the lath and grain boundaries of tempered martensite, where the C and Mn atoms tend to segregate.^[36] The supersaturated C in martensite in starting

microstructures partitioned into the intercritical austenite and also precipitated as carbide particles during the first stage of the IA treatment (Figures 5(b) and (c)).

Figure 6 shows some carbide particles at higher magnification and the diffraction pattern from an area containing one of these carbide particles, which is compatible with cementite. These cementite particles are almost completely dissolved after 15 min of IA and the volume fraction of RA increased up to 33 pct. Although the amount of austenite has doubled as the soaking time increases to 15 min, the carbon content of this phase has only been reduced by 0.26 pct due to the dissolution of the cementite particles. The rate of austenite formation for soaking times longer than 60 min dramatically decreased. For soaking times between 120 and 300 min, the RA content remains

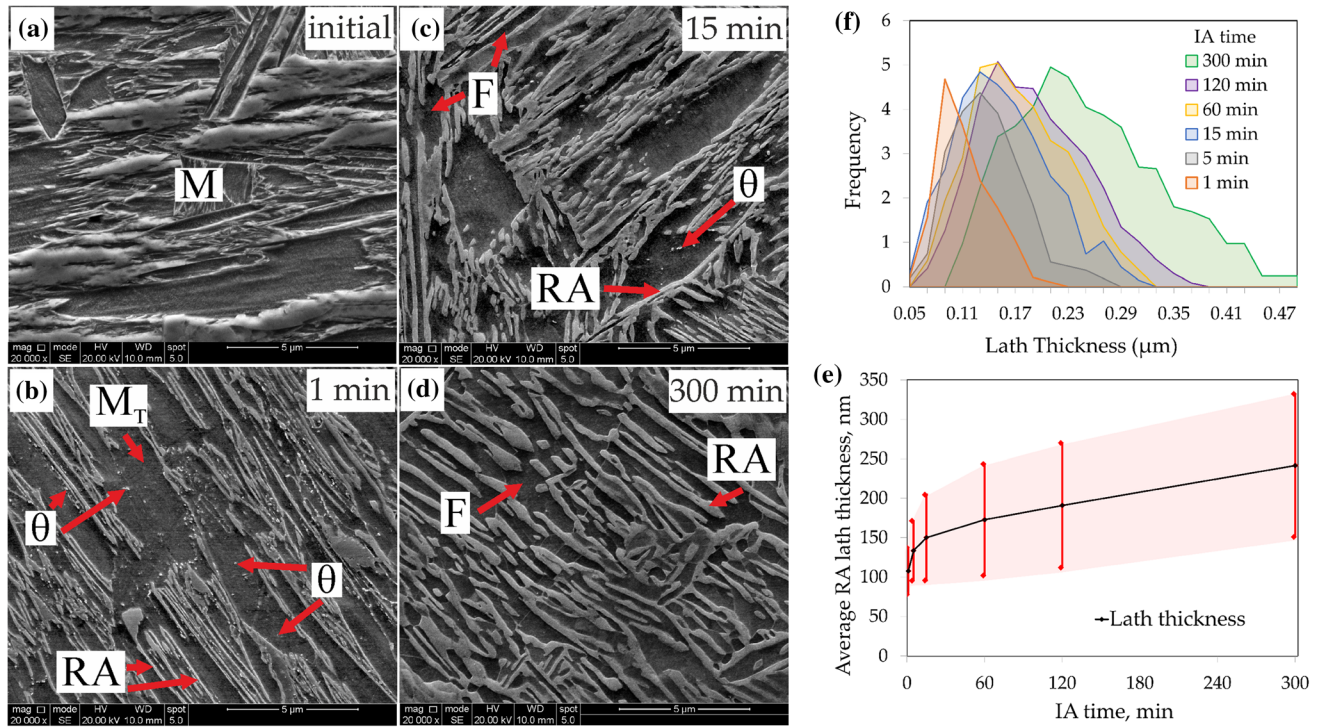


Fig. 5—SEM images of the microstructure present in (a) initial sample, after soaking at 680 °C for (b) 1 min, (c) 15 min, (d) 300 min, and evolution with soaking time of (e) average lath thickness and (f) frequency of thickness redistribution; RA – retained austenite; M – martensite; M_T – tempered martensite; F – ferrite; θ – carbides (Color figure online).

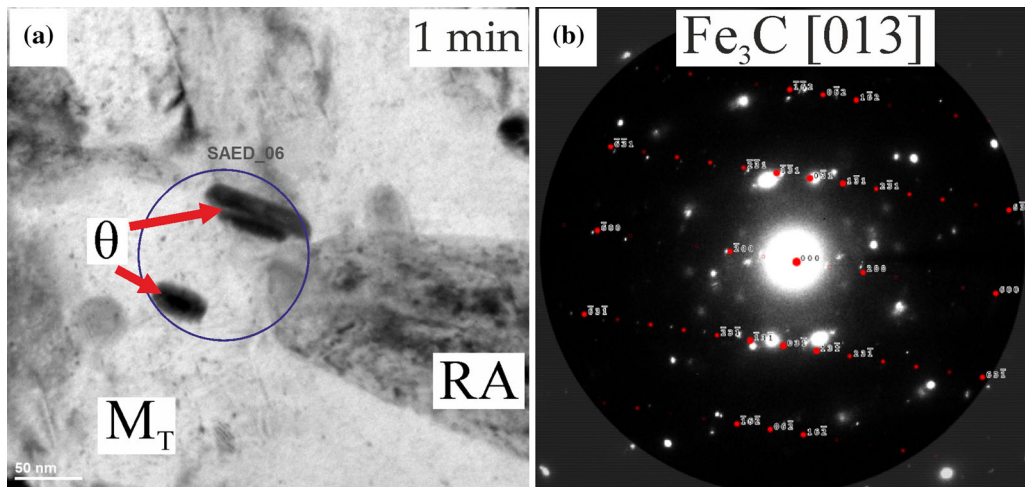


Fig. 6—TEM micrographs of the sample treated for 1 min (a) bright field image; (b) diffraction pattern from the area marked by a dark blue circle (Color figure online).

practically constant. Moreover, this longer holding time results in a clear fragmentation of thick ferritic laths, which leads to a homogeneous two-phase structure observed in Figure 5(d). This figure shows that increasing the soaking time results in an increase of the mean lath thickness of RA and a widening of the lath thickness distribution (Figure 5(e) and (f)). The most significant increase in the lath thickness (about 40 pct) occurs within the first 15 min of IA, with an average lath thickness increasing from 107 ± 30 to 150 ± 55 nm, when the soaking time is increased from 1 to after

15 min, respectively. Figure 4(e) shows an almost linear increase of the austenite lath thickness for longer soaking times, reaching a value of 240 ± 90 nm after 5 h. Wang and Van der Zwaag showed that decreasing the RA size increases the number of martensite nuclei needed to obtain a given martensite fraction and thus increases its stability.^[37] It is caused by RA boundaries acting as obstacles for martensite growth. In general, all produced microstructures show a very fine microstructure, which should stabilize RA much more than suggested from the calculated values of M_s

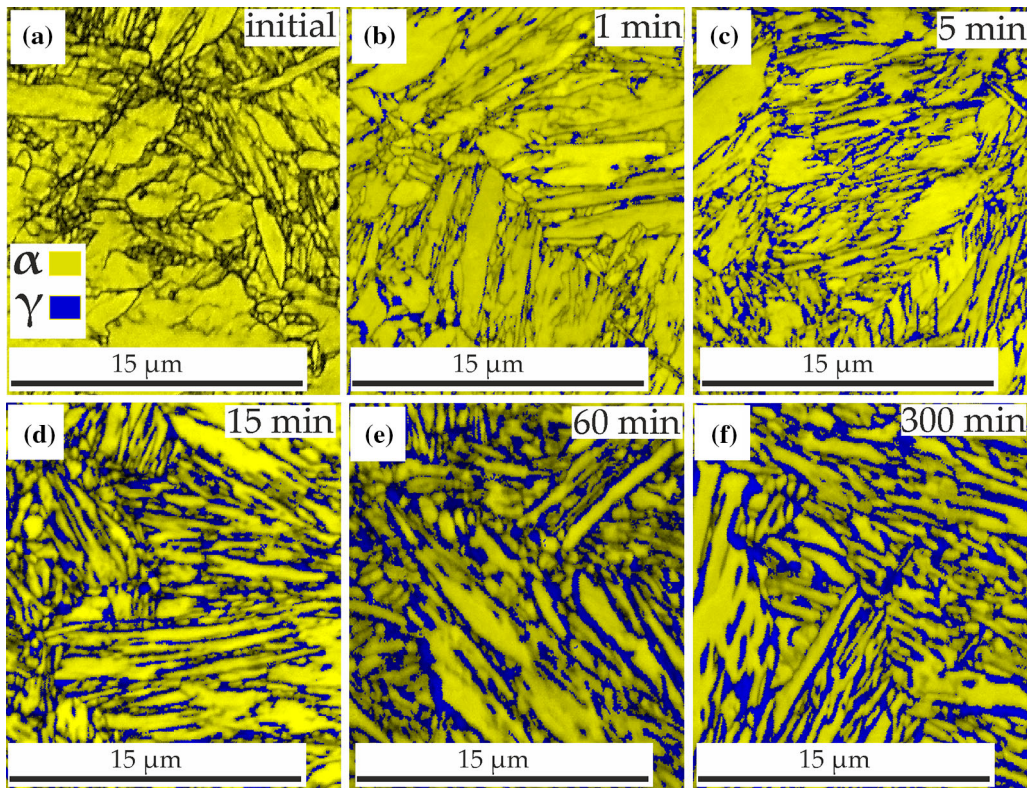


Fig. 7—EBSD phase maps for samples soaked for different times (Color figure online).

(Figure 2(c)). The increase in RA lath thickness and matrix tempering with soaking progress, however, are factors decreasing the relative RA stability slightly, which was evidenced by experimental M_s data measured for the treatment at 760 °C (Figure 3). The RA lath thickness evolution may also explain why the average enrichment of RA in Mn is so high just after 1 min of IA. The Mn enriches fast thin layers, where the diffusion distance in RA is short (Figure 4(a)). Further enrichment is inhibited by limited diffusion rate in thickening laths (Figure 5(e)), hence, the increase in the average Mn concentration slows down significantly as soaking time increases (Figure 2(b)). It should be noted that all samples with up to 120 min of IA contain some fraction of RA laths with a thickness of ≤ 50 nm (Figure 5(f)), while for the 300 min sample the smallest grains are > 100 nm thick. This may prove that new austenite grains nucleate almost during the entire applied soaking time, which results in a reduction and fragmentation of coarse ferritic grains as observed in the SEM images (Figure 5). The RA lath thickness distribution widens with increasing soaking time, which should positively affect the kinetics of SIMT and should allow an increase in the plasticity of the material by means of a gradual transformation of RA since the larger grains, less mechanically stable, will promptly transform to martensite at the beginning of plastic deformation, while the finer grains, more mechanically stable, will transform as further plastic deformation is applied.

EBSD analysis (Figure 7) indicates that austenite grains nucleate first at boundaries of martensitic laths.

With continued soaking, the austenite grows along the martensitic laths and starts to surround them and gets thicker as the RA fraction increases (Figures 7(b)-(f)). EBSD maps for samples treated for 1 and 5 min show an underestimated fraction of RA since the very thin < 50 to 70 nm austenite laths formed during the short process duration (Figures 5(b) and (f)) are not resolved by EBSD, since the surrounding phase interferes with their diffraction patterns leading to low IQ values at these locations. The grain misorientation (Figure 8(a)) distribution for the initial sample corresponds to that of a typical martensitic microstructure.^[38,39] There are visible peaks for low angle ($5 \text{ deg} >$) and high angle ($> 55 \text{ deg}$) boundaries related to increased dislocation density^[40] and mutual orientation of martensitic laths, respectively.^[38,39] With an increase in austenization time, the aforementioned peaks fade out (Figure 8(a)), while a fast increase in the number of grains with a misorientation of $\sim 45 \text{ deg}$ is visible (Figure 8(b)), which represent the α/γ orientation relationship.^[38] Based on the EBSD phase map (Figure 7) and misorientation results (Figure 8(b)) it can be assumed that each single ferritic grain is surrounded by RA with an average of 60 pct after 5 min of soaking and almost 80 pct after 5 h, ensuring a very homogeneous microstructure. This is a different relationship than in the case of IA after cold rolling, where both the ferrite and austenite grains are often located next to each other in a random manner.^[7,36] This tendency may influence the different mechanical behavior for both types of medium-Mn steels.

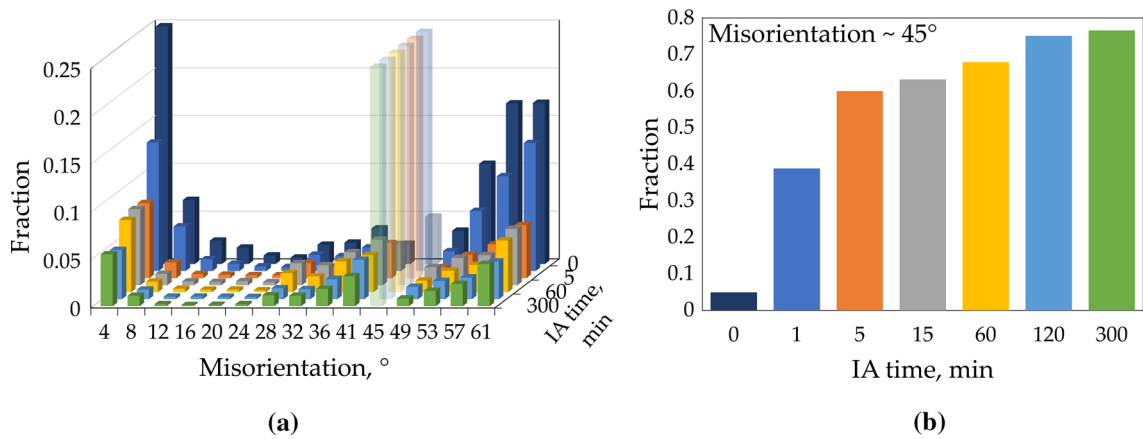


Fig. 8—EBSD results, (a) distribution of grain boundaries misorientation; and (b) fraction of grain boundaries with misorientation of $\sim 45^\circ$ (Color figure online).

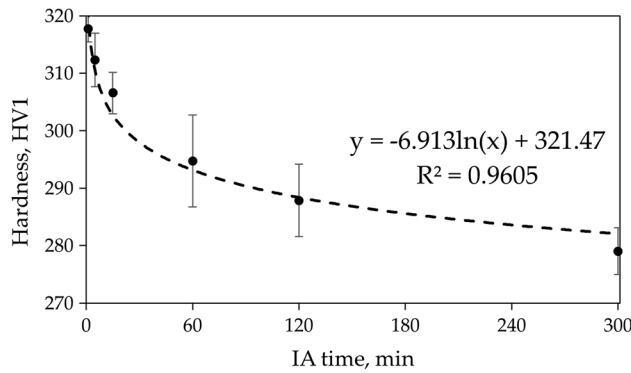


Fig. 9—Hardness (HV1) results of samples annealed for different times.

C. Mechanical Properties

In a steel, each phase present in the microstructure contributes to the overall mechanical properties of the aggregate. Thus, their hardness and tensile properties are determined by contribution of the matrix (ferrite, bainite, martensite or a combination of them) and the volume fraction, shape, and mechanical stability of austenite. All these microstructural parameters can be modified in a hot-rolled band plate by adapting the time and/or temperature used for the IA treatment, making possible the tailoring of the mechanical properties of these materials. The hardness of heat treated samples (Figure 9) decreases with prolonged austenitization time from 318 ± 10 HV1 after 1 min to 279 ± 8 HV1 after 5 h, which is related to martensite tempering and increase of the RA fraction. The same tendency is also observed in the reported YS values, which decrease from 859 ± 16 MPa to 591 ± 11 MPa for the same time range as above (Figure 10). Since the hardness and yield stress of the tempered martensite is higher than that of austenite, the average hardness values of the steel will decrease as the volume fraction of RA increases. The decrease of the UTS is much smaller than of the YS (from 938 ± 18 to 890 ± 20 MPa) due to intense SIMT in the samples soaked for more than 15 min. Such a result was anticipated as the prolonged soaking causes

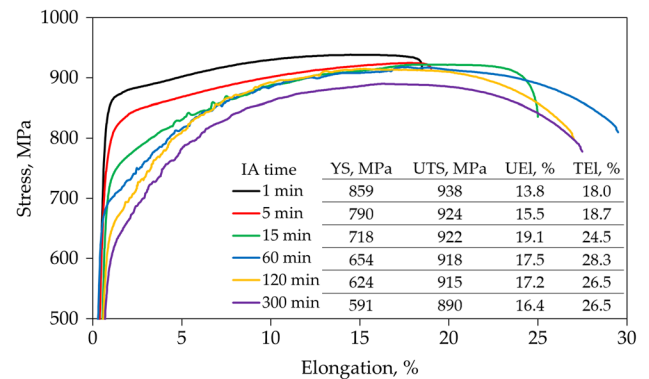


Fig. 10—Tensile test results of samples annealed for different times (Color figure online).

an increase in the fraction of RA with lower stability, whose transformation promotes an enhanced strain hardening.^[2] None of the samples exhibit discontinuous yielding due to the specific lath-like morphology. Both uniform elongation (UEL) and total elongation (TEL) (Figure 10) of the samples initially increase with increasing IA time demonstrating the highest UEL value of 19.5 ± 0.5 pct following a 15 min treatment and the highest TEL of 28.3 ± 0.6 pct following a 60 min treatment. Their ductility decreases slightly to final values of 16 ± 0.4 pct for UEL and 26.5 ± 0.8 pct for TEL after a treatment of 5 h.

For samples treated within 1 and 5 min the overall strain hardening is low due to remarkably high stability and corresponding low M_s temperatures, and thin laths ($< 110 \pm 30$ nm) of RA. Also, the RA in those samples is surrounded by tempered martensite, while in the rest of the samples the matrix is composed of ferrite. The high strength of the tempered martensite matrix further enhances RA stability.^[9] Therefore the influence of this factor should be the strongest in the sample treated for only 1 min. High RA stability in this sample is confirmed by the presence of 12 pct of this phase in the UEL region after tensile test (Figure 11). It means that RA exhibiting high stability does not transform even under

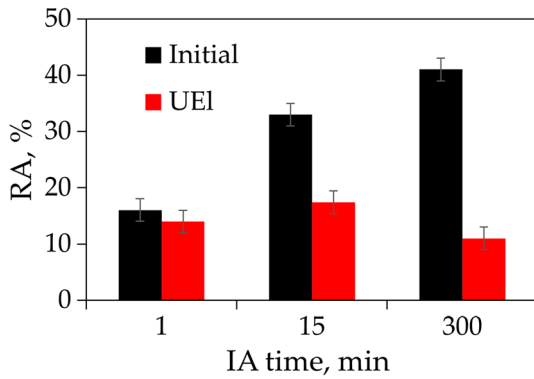


Fig. 11—The changes in RA fraction in the initial state and after deformation (measured in the UEL area) (Color figure online).

high strain.^[41] The sample treated for 15 min exhibits a relatively high and the most gradual strain hardening due to the most efficient SIMT. This sample has the highest UEL despite that only about half of the RA transformed to martensite under deformation (16.5 pct remains in microstructure). Its chemical stability and RA thickness characteristics are therefore considered as optimal among the investigated samples in terms of uniform elongation. For the longer soaking times, the RA transformation ratio reaches up to ~80 pct (Figure 11). However, the plasticity is limited due to massive SIMT in the early stages of deformation, as reflected in the very high strain hardening taking place up to 10 pct of sample elongation.^[42] This phenomenon is explained by the low mechanical stability of RA despite its calculated M_s being similar to the one of sample treated for 15 min, which is attributed to the thickest laths and the most tempered matrix among all samples. Therefore, in this case the increasing RA lath thickness and the degree of tempering of the matrix have a decisive influence on the stability of the RA. Those results show that the high fraction of RA does not guarantee high mechanical properties and that its stability (mainly controlled by lath thickness) is equally or even more important. This is also reflected in the fact that the sample containing 33 pct RA shows higher UEL due to higher stability of this phase than the sample containing 41 pct RA. This is important in terms of currently used mode of IA – batch annealing. For longer IA times, despite achieving the phase and chemical equilibrium (maximum RA fraction and its chemical stability), the matrix tempering and continuously increasing grain size/thickness lead to a decrease of the RA stability. A continuous IA focused on obtaining a high RA fraction by short annealing should be a research objective. The lower chemical stability of RA in such treatments would be substituted with a higher mechanical stability caused by thin RA laths and a less tempered matrix.

In order to describe the overall change in RA stability with the soaking time we can use again the tendency recorded for samples soaked at 760 °C (Figure 12). The martensitic transformation during cooling may be

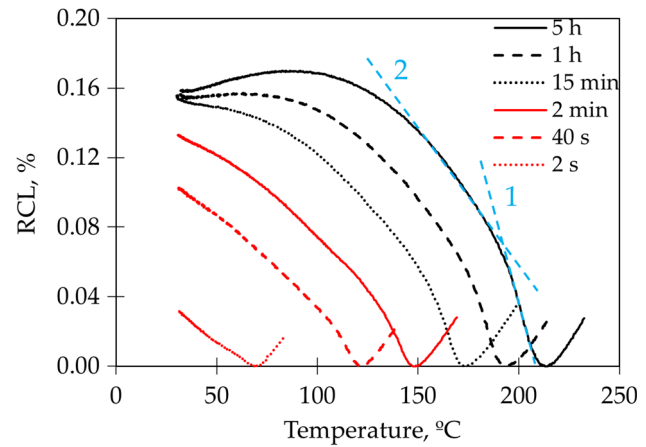


Fig. 12—Martensitic transformation kinetics during cooling for samples soaked at 760 °C for different time (Color figure online).

characterized by two factors: (1) the M_s temperature; and (2) transformation kinetics. The recorded curves shows that the M_s increases with the soaking time, *i.e.*, the transformation is “easier” to activate in samples treated for longer times. Additionally, a similar tendency applies to the kinetics of transformation itself. After longer soaking, the transformation is much more massive (Figure 12), which is especially visible at the beginning of transformation where the curve rises very steeply. It is caused by a higher austenite fraction in the microstructure, but also by its lower relative stability. Shorter soaking times result in less intense and more gradual transformation which is reflected by a more linear shape of the curve. The transformation kinetics during cooling may be transferred to the deformation conditions. The M_s temperature corresponds to the minimum strain, which activates the SIMT, while the austenite stability corresponds to SIMT kinetics. A high fraction of low stable austenite results in much stronger strain hardening at the beginning of deformation in samples treated for longer times, since SIMT starts at lower strains and is much more intense. A rapid increasing fraction of hard and brittle martensite of those samples makes it difficult to obtain increased plasticity (Figure 10). On the other hand, in samples treated for too short time, the SIMT needs higher strains to trigger the transformation and its kinetics are slower (reflected in high fraction of RA after deformation), which results in its low contribution to properties, and again limited plasticity. Therefore, it is important to achieve a compromise of both factors that will allow to obtain gradual SIMT over the entire range of deformation. The accurate description and analysis of deformation behavior requires a comprehensive approach to confirm the above analysis, which is the goal of the next stage of research. All recorded dilatometric curves of samples soaked at 760 °C (Figure 12) show that after the initial part of transformation its kinetics slows down slightly (marked by blue dashed lines on the 5 h curve). This characteristic is indicative of inhomogeneous

stability of RA. This phenomena is more intense for samples soaked for longer time and it may be caused by the heterogeneous Mn distribution, which was recorded for samples soaked at 680 °C (Figures 4(a) and (b)).

The results shows that the overall stability of RA decreases with increasing soaking time. It is influenced by C and Mn interplay in RA, its fraction, laths thickening and matrix tempering (this applies only to hot-rolled or austenized medium-Mn steels, as cold rolled ones undergo recrystallization during IA).^[7] The stability of the sample treated for 1 min is too high to contribute to SIMT (Figures 8 and 9), however, it indicates the possibility for further optimization process. The increase in IA temperature accelerates processes taking place during IA as shown by dilatometric results of samples soaked at 760 °C. In theory it should allow to obtain similar RA fraction during 1 min of soaking at higher temperature as in sample treated at 680 °C for 15 min or even 300 min. Its stability may be additionally improved for such short IA variant as the RA thickness in short process duration do not have time to get thicker (Figure 4(e)), and the martensite tempering may be limited. The performed investigations are a first step toward the continuous annealing of medium-Mn steels.

IV. CONCLUSIONS

The evolution of the microstructure and its mechanical properties accompanying the progress of intercritical annealing of an Al-containing medium-Mn steel was systematically studied as a function of the soaking time at 680 °C. It was found that:

1. At 680 °C all processes taking place during soaking (changes in the proportion of RA, its lath thickness, the redistribution of chemical elements) and thus the evolution of austenite stability are most dynamic in the first 15 min of IA.
2. A high fraction of RA obtained after a long IA time does not guarantee high mechanical properties as the shorter treated sample characterized by lower proportion of RA (< 8 pct) and higher mechanical stability showed the higher UEL.
3. The increase degree of matrix tempering and the RA thickening deteriorate the thermal and mechanical stability of samples soaked for longer times, limiting their mechanical performance.
4. After just 1 min soaking at 680 °C the alloy contains about 16 pct of lath-like RA, but its stability is too high to contribute to SIMT. However, it shows that short IA process times allow obtaining stable RA, which fraction and stability may be further optimized under conditions of high temperature continuous annealing.
5. The compromise of general chemical stability and its local distribution is needed to obtain gradual SIMT over the entire range of deformation, which in turn leads to the optimum combination of high strength and plasticity.

ACKNOWLEDGMENTS

The authors would like to thank MSc Krzysztof Matus for his contribution to the TEM investigations.

FUNDING

Adam Skowronek is a holder of European Union scholarship through the European Social Fund, grant InterPOWER (POWR.03.05.00-00-Z305). The publication was supported under the Initiative of Excellence—Research University program implemented at the Silesian University of Technology, 2022, Grant No. 32/014/SDU/10-21-02.

CONFLICT OF INTEREST

On behalf of all authors, the corresponding author states that there is no conflict of interest.

OPEN ACCESS

This article is licensed under a Creative Commons Attribution 4.0 International License, which permits use, sharing, adaptation, distribution and reproduction in any medium or format, as long as you give appropriate credit to the original author(s) and the source, provide a link to the Creative Commons licence, and indicate if changes were made. The images or other third party material in this article are included in the article's Creative Commons licence, unless indicated otherwise in a credit line to the material. If material is not included in the article's Creative Commons licence and your intended use is not permitted by statutory regulation or exceeds the permitted use, you will need to obtain permission directly from the copyright holder. To view a copy of this licence, visit <http://creativecommons.org/licenses/by/4.0/>.

REFERENCES

1. P.J. Gibbs: Thesis, Colorado School of Mines. Arthur Lakes Library, 2014.
2. I. Janeiro, O. Hubert, and J.-H. Schmitt: *Int. J. Plast.*, 2022, vol. 154, 103248.
3. W. Wang, Y. Liu, Z. Zhang, M. Yang, L. Zhou, J. Wang, P. Jiang, F. Yuan, and X. Wu: *Mater. Sci. Technol.*, 2023, vol. 132, pp. 110–18.
4. D. Raabe, H. Springer, I. Gutierrez-Urrutia, F. Roters, M. Bausch, J.B. Seol, M. Koyama, P.-P. Choi, and K. Tsuzaki: *JOM*, 2014, vol. 66, pp. 1845–56.
5. A. Grajcar, P. Skrzypczyk, and D. Wozniak: *Arch. Metall. Mater.*, 2014, vol. 59, pp. 1691–97.
6. Y. Li, D.S. Martin, J. Wang, C. Wang, and W. Xu: *Mater. Sci. Technol.*, 2021, vol. 91, pp. 200–14.
7. Y.-K. Lee and J. Han: *Mater. Sci. Technol.*, 2015, vol. 31, pp. 843–56.
8. C. Liu, F. Xiong, G. Liu, Y. Wang, Y. Cao, Z. Xue, and Q. Peng: *Materials*, 2021, vol. 14, p. 7132.
9. J. Hidalgo, K.O. Findley, and M.J. Santofimia: *Mater. Sci. Eng. A*, 2017, vol. 690, pp. 337–47.

10. K. Davut and S. Zaefferer: *Mater. Res. Soc. Sympos. Proceedings*, <https://doi.org/10.1557/opl.2011.1447>.
11. A. Ito, A. Shibata, and N. Tsuji: *Mater. Sci. Forum.*, 2016, vol. 879, pp. 90–94.
12. A. Grajcar, A. Kilarski, A. Kozłowska, and K. Radwański: *Materials*, 2019, vol. 12, p. 501.
13. S. Kaar, K. Steineder, R. Schneider, D. Krizan, and C. Sommitsch: *Scr. Mater.*, 2021, vol. 200, 113923.
14. A. Skowronek, A. Grajcar, A. Kozłowska, A. Janik, M. Morawiec, and R.H. Petrov: *Metall. Mater. Trans. A*, 2022, vol. 53A, pp. 3012–21.
15. H. Huang, O. Matsumura, and T. Furukawa: *Mater. Sci. Technol.*, 1994, vol. 10, pp. 621–26.
16. F. Wang, X. Ye, S. Ren, K. Zhang, X. Liang, and G. Liu: *Materials*, 2022, vol. 15, p. 2425.
17. M. Haupt, A. Dutta, D. Ponge, S. Sandlöbes, M. Nellessen, and G. Hirt: *Proc. Eng.*, 2017, vol. 207, pp. 1803–08.
18. P.J. Gibbs, E. De Moor, M.J. Merwin, B. Clausen, J.G. Speer, and D.K. Matlock: *Metall. Mater. Trans. A*, 2011, vol. 42A, pp. 3691–3702.
19. A. Arlazarov, M. Goune, O. Bouaziz, A. Hazotte, and F. Kegel: *Materials Science Forum*, Trans Tech Publications, Quebec, 2011, pp. 706–09.
20. D.-W. Suh, S.-J. Park, T.-H. Lee, C.-S. Oh, and S.-J. Kim: *Metall. Mater. Trans. A*, 2010, vol. 41A, pp. 397–408.
21. M. Morawiec and A. Grajcar: *Achiev. Mater. Manuf.*, 2017, vol. 1, pp. 11–17.
22. N. van Dijk, A. Butt, L. Zhao, J. Sietsma, S. Offerman, J. Wright, and S. Zwaag: *Acta Mater.*, 2005, vol. 53, pp. 5439–47.
23. H. Steven and A.G. Haynes: *J. Iron Steel Institute*, 1956, vol. 183, pp. 349–59.
24. D. Barbier: *Adv. Eng. Mater.*, 2014, vol. 16, pp. 122–27.
25. L. Samek, E. De Moor, J. Penning, and B.C. De Cooman: *Metall. Mater. Trans. A*, 2006, vol. 37A, pp. 109–24.
26. J. Hidalgo, C. Celada-Casero, and M.J. Santofimia: *Mater. Sci. Eng. A*, 2019, vol. 754, pp. 766–77.
27. Q. Guo, H.-W. Yen, H. Luo, and S.P. Ringer: *Acta Mater.*, 2022, vol. 225, 117601.
28. S.-J. Lee, S. Lee, and B.C. De Cooman: *Scr. Mater.*, 2011, vol. 64, pp. 649–52.
29. A. Marceaux, D. Clément, K. Hoummada, J. Drillet, V. Hebert, and P. Maugis: *Comput. Mater. Sci.*, 2020, <https://doi.org/10.1016/j.commatsci.2020.109786>.
30. L. Král, B. Million, and J. Čermák: *Defect Diffus Forum*, 2007, vol. 263, pp. 153–58.
31. R.S. Varanasi, M. Lipińska-Chwałek, J. Mayer, B. Gault, and D. Ponge: *Scr. Mater.*, 2022, vol. 206, 114228.
32. B. Hu, X. Shen, Q. Guo, Q. Wen, X. Tu, C. Ding, F. Ding, W. Song, and H. Luo: *Mater. Sci. Technol*, 2022, vol. 126, pp. 60–70.
33. N. Nakada, K. Mizutani, T. Tsuchiyama, and S. Takaki: *Acta Mater.*, 2014, vol. 65, pp. 251–58.
34. S. Lee, S.-J. Lee, S. Santhosh Kumar, K. Lee, and B.C.D. Cooman: *Metall. Mater. Trans. A*, 2011, vol. 42A, pp. 3638–51.
35. J. Speer, R. Rana, D. Matlock, A. Glover, G. Thomas, and E. De Moor: *Metals*, 2019, vol. 9, p. 771.
36. J. Han, S.-J. Lee, J.-G. Jung, and Y.-K. Lee: *Acta Mater.*, 2014, vol. 78, pp. 369A–77.
37. J. Wang and S. Van Der Zwaag: *Metall. Mater. Trans. A*, 2001, vol. 32, pp. 1527–39.
38. S. Zajac, V. Schwinn, and K.-H. Tacke: *Mater. Sci. Forum.*, 2005, vol. 500–501, pp. 387–94.
39. A. Kajjalainen, M. Liimatainen, V. Kesti, J. Heikkala, T. Liimatainen, and D. Porter: *Metall. Mater. Trans. A*, 2016, vol. 47, pp. 4175A–88.
40. N.P. Gurao and S. Suwas: *Sci Rep*, 2014, vol. 4, p. 5641.
41. Y. Zou, Y.B. Xu, D.T. Han, Z.P. Hu, R.D.K. Misra, L.F. Cao, and H. Song: *Mater. Sci.*, 2019, vol. 54, pp. 3438–54.
42. Y. Ma, W. Song, S. Zhou, A. Schwedt, and W. Bleck: *Metals*, 2018, vol. 8, p. 357.

Publisher's Note Springer Nature remains neutral with regard to jurisdictional claims in published maps and institutional affiliations.